Cloud Publications
International Journal of Advanced Remote Sensing and GIS
2016, Volume 5, Issue 2, pp. 1539-1560
ISSN 2320 - 0243, Crossref: 10.23953/cloud.ijarsg.77

Methodology Article **Open Access**

Assessment of Land Degradation Status and Its Impact in Arid and Semi-Arid Areas by Correlating Spectral and Principal Component Analysis Neo-Bands

Alfred Homère Ngandam Mfondoum[1,3], Joachim Etouna[2,3], Buji Kindess Nongsi[3,4], Fabrice Armel Mvogo Moto[3,4], and Florine Gustave Noulaquape Deussieu[3,4]

[1] Laboratory of Natural Resources Management, Department of Geography, University of Yaoundé I, Cameroon
[2] Laboratory of Remote Sensing and Spatial Analysis, National Institute of Cartography, Yaoundé, Cameroon
[3] Technical Committee of Geospatial Techniques, ILG Asso., Centre of Handicapped Street, Yaoundé, Cameroon
[4] Master's Research Unit of Remote sensing and GIS Applied to Territorial Planning, Department of Geography, University of Yaoundé I, Yaoundé, Cameroon

Publication Date: 22 February 2016

DOI: https://doi.org/10.23953/cloud.ijarsg.77

Copyright © 2016 Alfred Homère Ngandam Mfondoum, Joachim Etouna, Buji Kindess Nongsi, Fabrice Armel Mvogo Moto, and Florine Gustave Noulaquape Deussieu. This is an open access article distributed under the **Creative Commons Attribution License**, which permits unrestricted use, distribution, and reproduction in any medium, provided the original work is properly cited.

Abstract This paper aimed to assess the status of land degradation in arid and semi-arid areas based on a correlation analysis between spectral and statistical neo-bands. The methodology uses vegetation and soil spectral indices as the second Modified Soil Adjusted Vegetation Index (MSAVI2), Normalized Difference Bare Soil Index (NDBSI), Texture Index (NDTeI), Crust Index (CI), Top Soil Grain Size Index (GSI), Normalized Difference Sand Dune Index (NDSDI) and the first Specific Principal Component of the red, near infrared, shortwave infrared bands stacking ($SPC1_{R\text{-}NIR\text{-}SWIR1\text{-}SWIR2}$). The vegetation is considered here as the main object of soil sub-surface. Thus after all the spectral and the statistic neo-bands are performed on Landsat8 OLI sensor image, a linear regression is generated to assess their correlation with MSAVI2. Based on the visual interpretation and the regression curves the results show that the determination coefficient R^2 and the P values all significant as less than 0.0001. Each neo-band is weighted with its R^2 to improve its contribution to the model and the synthesis image obtained enhances the land degradation sensing in six classes; these are respectively named as ''severe'' (3139 km^2), ''high'' (6763 km^2), ''moderate'' (8341 km^2), ''low'' (7454 km^2), ''very low'' (6947 km^2) and ''close to nil'' (5437 km^2). This last image is summed with population layer to produce a decision map helpful for further government decision. At the end the degradation image has given interesting results for the detection of land degradation comparatively to derivation and comparison of individual indices.

Keywords *Correlation Analysis; Decision Map; Linear Regression; Specific Principal Component; Spectral Indices*

1. Introduction

Land degradation refers to a change in soil health condition that causes a reduction in the ecosystem's ability to provide goods and services for its beneficiaries (Barrow, 1991; Conacher and Sala, 1998; Biancalani, n.y.). It is also defined as the loss of soil production by either chemical or physical processes (Singer and Munns, 2002; Blaikie and Brookfield, 1987). It thus covers the various types of soil degradation as physical, chemical and biological (Brabant, 2010), adverse human impacts on water resources, deforestation, and lowering of the productive capacity of rangelands (Metternicht, 2006; UNEP, 1992). Brabant (2009) testify that fighting this process is now a priority, particularly in developing countries which host 75% of the world's population and where 3/4 people work in agriculture; but the main obstacle to achieve such evaluations has been the lack of a standard streamlined international assessment procedure. Further, the UNCCD (1994) and Fadhil (2009) have listed several biophysical but also socio-economic causes to that phenomenon as marketing, income, human health, institutional support, poverty, undermining food production and political stability. From a holistic point of view and in its extreme form, land degradation is followed by a severe deterioration of vegetation cover and soil production capacity reduction takes the connotation of desertification, particularly in those semi-dry arid or arid areas (Warren and Agnew, 1988; Begzsuren, 2007).

Assuming the importance of land in several scientific fields it is necessary to know the actual and available tools belonging to the field of remote sensing and GIS, in order to assess the early detection of "Soil Degradation" or to take up any preventive measures (Rojas, 2013). Several studies and models have been devoted to the prediction of erosion risk based on the USLE (Universal Soil Loss Equation) of Wischmeier and Smith (1978), and the RUSLE (Revised Universal Soil Loss Equation of (Renard et al., 1991). Concerning the analysis of the state of land degradation it is encouraged and supported by projects such as LADA (Land Degradation in Drylands Assessment) which aims to develop an integrated assessment methodology for land degradation to understand the degradation processes at different scales (global, national and local) by identifying the status and trends of land degradation, the root causes, effects and consequences. On that point of view, MSAVI has been used in correlation with field data to assess vegetation cover (Senseman et al., 1996a; Senseman et al., 1996b; Chen, 1999), biomass and/or leaf area index (Smith et al., 2005; Phillips et al., 2009), or as one indicator to monitor desertification (Liu and Wang, 2005). Pandey et al. (2013) have used some spectral indices such as CI (Crust Index), NDSDI (Normalized Difference Sand Dune Index), GSI (Top Soil Grain Size Index) compare to NDVI (Normalized Difference Vegetation Index) to assess land degradation and sand encroachment in Western India. Also, Raina et al. (1991) have used Landsat TM imagery to map the type, extent and degree of degradation. The soils affected by fires and their capacity for regeneration has been studied from images Landsat TM and Digital Elevation Model (DEM) (González and Rodríguez, 2013).

Based on these applications and experimentations, the main objective of this article is to assess the state of land degradation through the correlation analysis of vegetation and soils spectral indices, and SPC neo-band, followed by their crossing.

2. Research Location

The area chosen for this study is the far-north of Cameroon in Central Africa. It is situated between the longitude 13˚30'-15˚40' East and longitude 10˚-13˚ North (Figure 1). It covers a total area of about 38086 km^2 and six departments are concerned. Several reasons explain this choice. This is indeed a bioclimatic milieu naturally predisposed to several forms of soils damages due to the dry hot climate and low rainfall. As consequences vegetation cover gradually changes from weak dense grassy savannah in the south to very sparse dry savannah or steppe as one moves in latitude. The soils are typically arid including ferruginous, alluvial, sandy, also latosols and vertisols, all barren and yellowish, skeletal and therefore poor (Raunet, 1993).

In addition the 3,300,324 inhabitants (BUCREP, 2010) of the area are facing landholding conflicts and live from agriculture and transhumant breeding with some practices as bushfire and irrigation by pumping or pouring (MINEF-UNCCD, 2004; COMIFAC-CEEAC, 2007). All these bioclimatic and human characteristics expose the concern area to many forms of land degradation such as rock levelling, gullying, valleys silting, banks sapping, wind and water erosion, the extension of dune banks, drying and induration due to cattle trampling, armoring or crusting (Figure 2). In 2003 the GLADA was estimating the total of degraded area in Cameroon to 151605 km^2 which represent 31.89% of national territory (Bai et al., 2008).

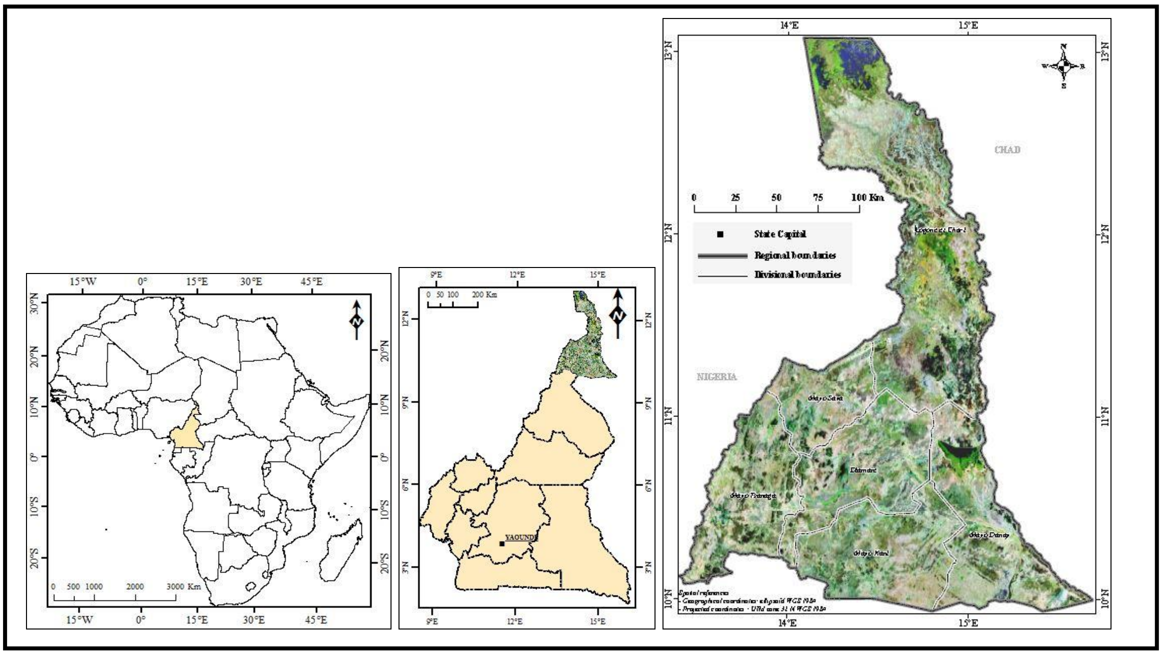

Figure 1: *The Study Area in Background of Landsat Image Bands Composition 5-4-3*

Mountainous Rock Levelling

Bare and Burned Fallow Lands

Gullying

Valley Silting

Cattle Trampling

Bank Sapping

Figure 2: *Some Features of Land Degradation*

3. Materials and Methods

3.1. Satellite Image Acquisition and Preprocessing

Satellite images of Landsat 8 OLI sensor were downloaded at the middle of the dry season, characterized by the absence of rainfall and very slow chlorophyll activity; thus implicitly declining agricultural activities. This is a total of seven scenes acquired on January 2015, on the official website of NASA http://earthexplorer.usgs.gov/ (Table 1). Each scene is composed by eleven bands covering the electromagnetic spectrum between 0.433 µm and 12.50 µm. The bands stacked are blue, green, red, near infrared, and the two shortwave infrared with a spatial resolution of 30 meters, while the panchromatic band is at 15 meters (Table 2).

Table 1: *List of Scenes used*

Scene ID	Date of Acquisition
LC81830532015014LGN00	14/01/2015
LC81840512015021LGN00	21/01/2015
LC81840522015021LGN00	21/01/2015
LC81840532015005LGN00	05/01/2015
LC81850512015012LGN00	12/01/2015
LC81850522015012LGN00	12/01/2015
LC81850532015028LGN00	28/01/2015

Table 2: *Spectral and Spatial Characteristics of Bands Used*

Spectral Band	Wavelength (µm)	Spatial Resolution (M)
Aerosol / Coastal	0.433 - 0.453	30
Blue	0.450 - 0.515	30
Green	0.525 - 0.600	30
Red	0.630 - 0.680	30
Near Infrared	0.845 - 0.885	30
Short Wavelength Infrared	1.560 - 1.660	30
Short Wavelength Infrared	2.100 - 2.300	30
Panchromatic	0.500 - 0.680	15

Preprocessing operations were performed to prepare the images. This step starts by the radiometric calibration and atmospheric corrections by Chavez (1996) low COST method on each scene. Then a spatial enhancement to 15m has been applied to merge the multispectral image with the panchromatic band. The process used has been the wavelet resolution merge that can be considered as an improvement of the classical IHS (Intensity Hue Saturation) method and it is expected to better preserve the spectral characteristics of the multispectral image (Ferreres et al., no year). It processes the signals of the image as the Fourier Transform for better readability of a phenomena and uses short discrete "wavelets" instead of a long wave (King and Wang, 2001; ERDAS, 2003; Klonus and Ehlers, 2009; Zaydan, 2012). Finally, the entire data set of seven scenes was mosaicked and clipped to the limits of the study area as the final step in the preprocessing sequence.

2.2. Presentation of Spectral Indices Generated

Spectral indices have proved efficiency to highlight the indicators of land degradation mentioned above. Applications of remote sensing for assessing and monitoring land degradation is mainly related to spectral reflectance of soil and vegetation (Al-Bakri, 2012). The approach used here has been implemented using two entrances.

The first entrance is the characterization of the land surface cover through a vegetation density index. Indeed the determination of soil recovery rate by vegetation is a fundamental indicators to measure soil protection rate (Deschamps, 1983). So far the most frequently used method employing EO datasets is trend analysis of vegetation index data, most commonly the Normalized Difference Vegetation Index (NDVI) (Higginbottom and Symeonakis, 2014). In this study, the Second Modified Soil-Adjusted Vegetation Index, MSAVI2 of (Qi et al., 1994) has been used. This index describes the state and the density of the vegetation while separating it from the ground effects especially when the canopy is sparse and Leaf Area Index, LAI, is low (Table 3, Figure 5a). It is advantageous in the assessment of the top soil elements on arid and semi-arid surfaces according to the formula (1):

$$\mathrm{MSAVI2} = \frac{(2 * NIR + 1 - \sqrt{(2 * NIR + 1)^2 - 8 * (NIR - R)})}{2} \quad (1)$$

Where NIR and R, are respectively values of reflectance in the near infrared (band 5: 0845-0885 µm) and Red (band 4: 0630-0680 µm) electromagnetic spectrum.

The second entrance has been that to characterize the state of topsoil cover. It then important to remember that apart from the degree of coverage by vegetation, soil reflectance is influenced by intrinsic factors such as moisture, roughness (Barnes and Zalewski., 2003; Thomasson et al., 2001) stoniness, microrelief and texture thinness (Madeira et al., 1991; Touriño Soto, 2005). It is admitted that the most important interaction of soils and electromagnetic radiation is in the range of 0.3 to 3 µm (Zaydan, 2012). Then in arid and semiarid areas, spectral reflectance of soil is mainly controlled by the dominant particle size and the content of minerals, including accumulated salts (Al-Bakri, 2012). Five indices and one statistical neo-band were chosen to highlight these factors:

- The Normalized Difference Bare Soil Index, NDBSI, aims at enhancing bare soil areas, fallow lands, and vegetation with marked background response. It is a normalized difference using the Near and the Short wavelength infrared as follows in formula (2):

$$NDBSI = \frac{SWIR - NIR}{SWIR + NIR} + 0{,}001 \quad \in [-1, 1] \quad (2)$$

Where SWIR refers to the reflectance values in the short wavelength infrared (band 6: 1560-1660 µm) Landsat OLI sensor. It is useful for predicting and assessing bare soil characteristics such as roughness, moisture content, amount of organic matter, and relative percentages of clay, silt, and sand (Roy et al., 1997) (Table 3). In general condition NDBSI > −0.20 is a strong necessary, but not sufficient indication of the presence of bare soil areas (Baraldi et al., 2006).

- The normalized difference between the two bands of the Short Wavelength infrared, important to enhance the contrast of texture or roughness of tropical soils. It was originally used to express the content of gibbsite and kaolinite in latosoils, and therefore allows to distinguish the sandy soils from clay soils in tropical areas (Madeira, 1993). It particularly enhance clay soils, sandy soils, rocks leveling, vertisoils and latosoils in tropical areas under or over the vegetation as it is the case in the study area (Table 3). It will be named in this study the Normalized Difference Texture Index, NDTeI, that uses the spectral domain of the infrared with the formula (3):

$$NDTeI = \frac{SWIR1 - SWIR2}{SWIR1 + SWIR2} \quad \in [-1, 1] \quad (3)$$

Where SWIR2 is the reflectance values the second Short Wavelength infrared Landsat OLI sensor (band 7: 2100-2300 µm).

- The Topsoil Grain Size Index, GSI, is used to characterize the surface texture of the soil. Taking in account the fact that soil physical degradation involves thinning of the organic layer, destabilization of aggregate structure in the topsoil, surface crusting and topsoil compaction (Brabant et al., 1996), this index is increasingly coupled to vegetation indices to indicate degradation, based on the fact that the increase in this index is indicative of a rough surface texture (Xiao et al., 2006) (Table 3). The higher values indicate that the soil is coarse and close to degradation. The formula (4) is based on the reflectance values of the spectral bands of the visible as follow :

$$GSI \frac{R-B}{R+B+G} \qquad (4)$$

Where B and G express the reflectance values in the blue band (band 2: 0450-0515 µm) and the green band (0525-0600 µm) OLI Landsat sensor. GSI value is close to 0 or a smaller value in vegetated area, and for a body of water it is a negative value. Higher positive values of GSI represent the sand affected region.

- The Crust Index, CI, is a normalized difference between the red and blue domain of electromagnetic spectrum. It is mainly used to map geological features, and has the ability to detect and differentiate lithological/morphologic units such as active crusted sand areas (Karnieli, 1997) (Table 3). The formula of the CI is:

$$CI = 1 - \left(\frac{R-B}{R+B}\right) \in [0, 1] \qquad (5)$$

- The Normalized Difference Sand Dune Index, NDSDI, is used to identify and assess the existence of the sand dune accumulations and sand spread (Fadhil, 2009). This normalized difference is calculated between the Red and the short wavelength infrared (SWIR) spectral values following the formula (6):

$$NDSDI = \frac{R-SWIR2}{R+SWIR2} \in [-1, 1] \qquad (6)$$

This index mainly distinguishes vegetation and non-vegetation, water and arid surface, sandy or bare soil, while reflectance in the red and SWIR bands can discriminate the mineral and rock types as it is sensitive to the moisture content of soil and vegetation (Table 3). Value of the NDSDI ranges between -1 and +1, whereas the sand dune accumulations and drifting sands often give values below zero and vegetative cover produces values greater than zero.

- The first Selective Principal Component R-NIR-MIR-SWIR: the Principal Component Analysis (PCA) also named Hotelling transform is a mathematical transformation used in remote sensing to develop the image signal on the basis of orthogonal functions of these (Bonn et al., 1992; Joly, 1986; Baccini, 2010; Gonzalez, no year). It looks for a better representation of numerous information, n, in a sub-space F_k in space R_p of k dimension. Thus k new variables which are linear combinations of p initial variables and that minimize the loss of information are defined (Figure 3).

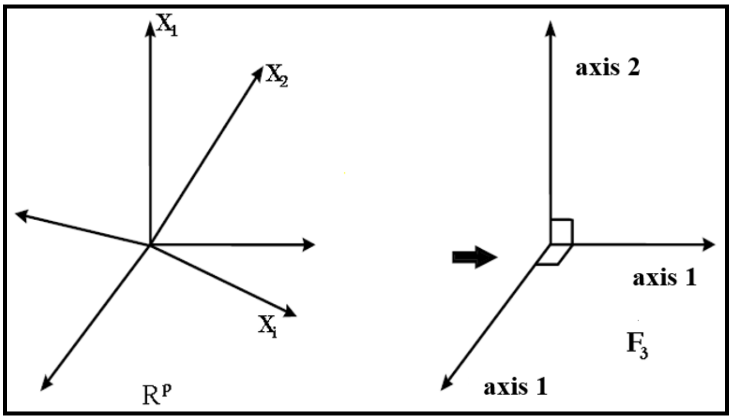

Figure 3: *Schematic Explanation of the PCA [Smith et al., 2005]*

This technique works to search axes larger variances in the space of radiometry of an image (Youan, 2009). Some authors have derived the selective principal component, SPC, to enhance lithological lineaments. The bands of the visible and the ones of the infrared part of the electromagnetic spectrum are compiled separately to produce the selective principal component of blue-green-red, SPC_{BGR} and the selective principal component of near infrared-shortwave infrared one and two, $SPC_{NIR-SWIR1-SWIR2}$. Then the first SPC of the results is chosen to proceed with the analysis. In this study the $SPC_{R-NIR-SWIR1-SWIR2}$ have been used to generate new axes of images information; this is according to the fact that the red band coupled to the NIR easily separate soils from vegetation; while the spectral curve of soil is more distinct in the infrared domain (Figure 4).

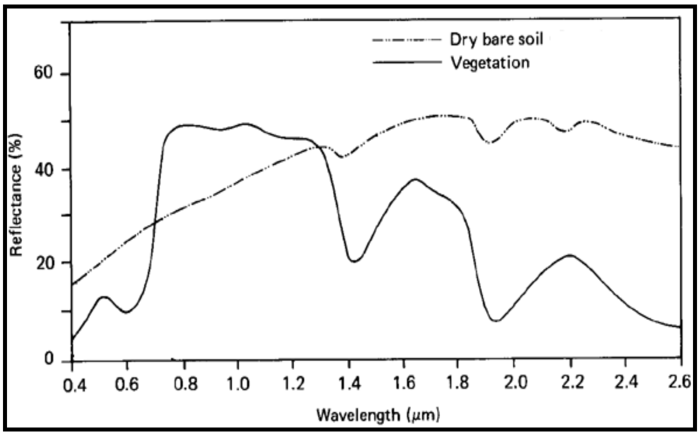

Figure 4: *Generalized Spectral Signatures for Soil and Vegetation*
(Source: Wageningen University)

With an eigenvalue of 21870.68 over 22016.39, that is an explained variance of 99, 33 %, the $SPC1_{R-NIR-SWIR1-SWIR2}$ concentrates the essential of information contained in the four bands and has been selected to continue the process. Then the soil surface characteristics enhanced are rough lithological features considered as a part of land degradation (Table 3).

Table 3: *Contribution of Neo-Bands Used To the Detection of Degraded Lands*

Neo-Bands	Main Contribution To Degraded Lands Detection	Significant Values And Threshold	
		≤ 0	> 0
MSAVI2	Vegetation density	Absence of vegetation	Presence of vegetation
NDBSI	bareness, roughness, fallow lands ;	Absence of Bare soil (< -0.20)	Presence of bare soil (> -0.20)
NDTeI	Soil surface texture, roughness;	Low texture and roughness	High texture and roughness

CI	Actives encrusting	Low encrusting	High encrusting
GSI	Sand and rocks grains size, stoniness, surface texture	Body of water (<0); vegetated area (=0)	Sand affected area and bare soil surface
NDSDI	Sandbank, sand spread, dune accumulation, drifting sands	Sand dune accumulations, drifting sands;	Vegetative cover
SPC1$_{R\text{-}NIR\text{-}SWIR1\text{-}SWIR2}$	Rough and lithological elements of top soil	Non-significant	Important

2.3. Experimentations

2.3.1. Calculation of Indices Correlations

Two indices are considered equivalent if the decision made on the basis of one index could have been made equally well on the basis of the other index (Perry and Lautenschlager, 1984). Moreover binary discrimination between classes of vegetation and non-vegetation requires at least a pair of indexes, to guarantee separability of these two land cover types in feature space (Baraldi et al., 2006). Thus the six indices and the PCA have been generated through the Erdas imagine 2014 software model maker (Figure 5).

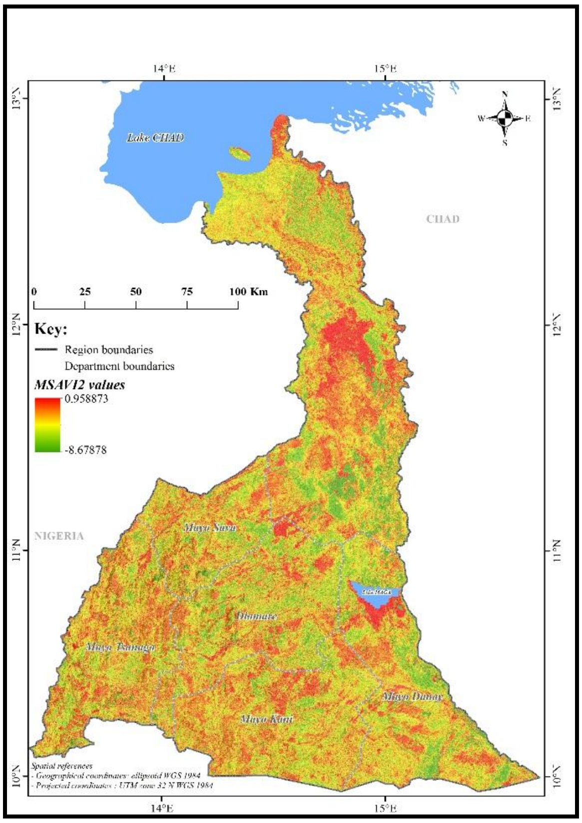

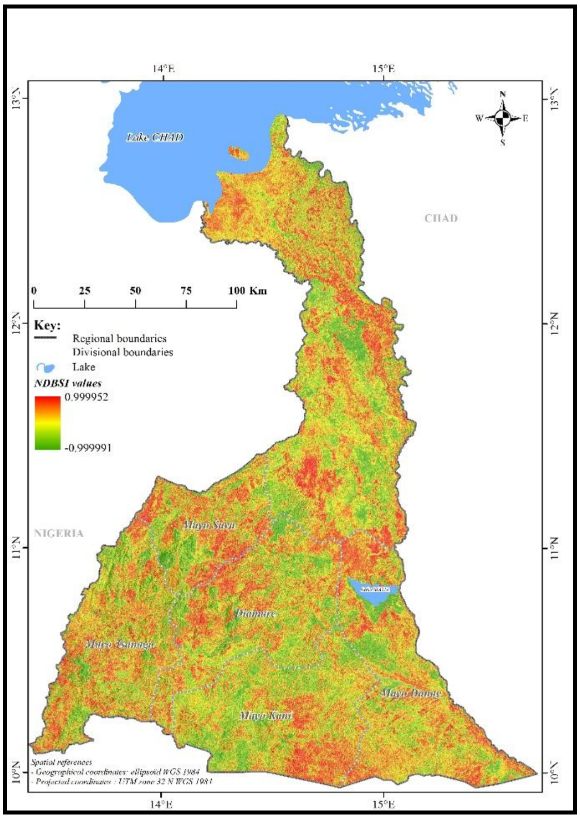

Figure 5a: *MSAVI2 (i)* *NDBSI (ii)*

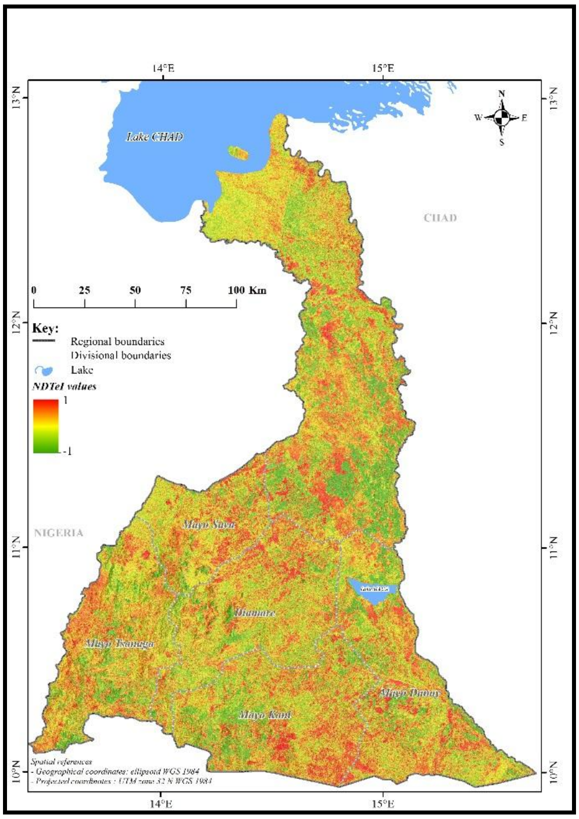

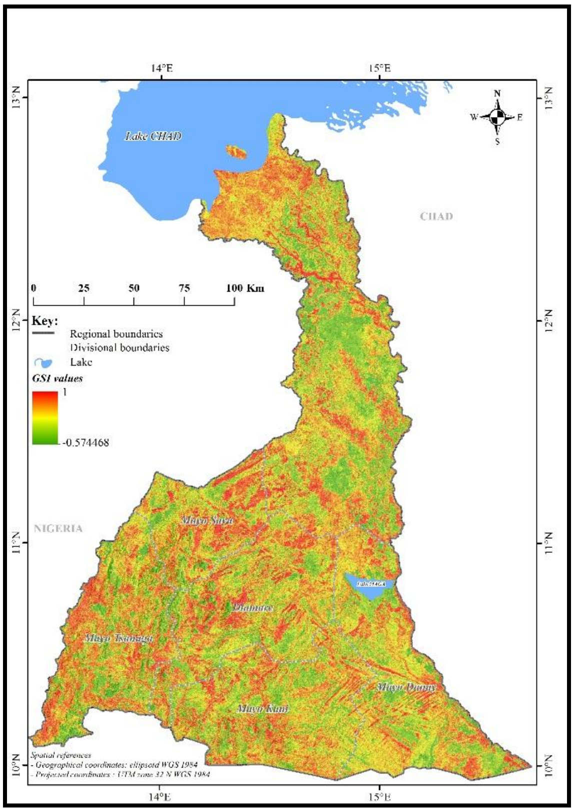

Figure 5b: *NDTeI (iii)* *GSI (iv)*

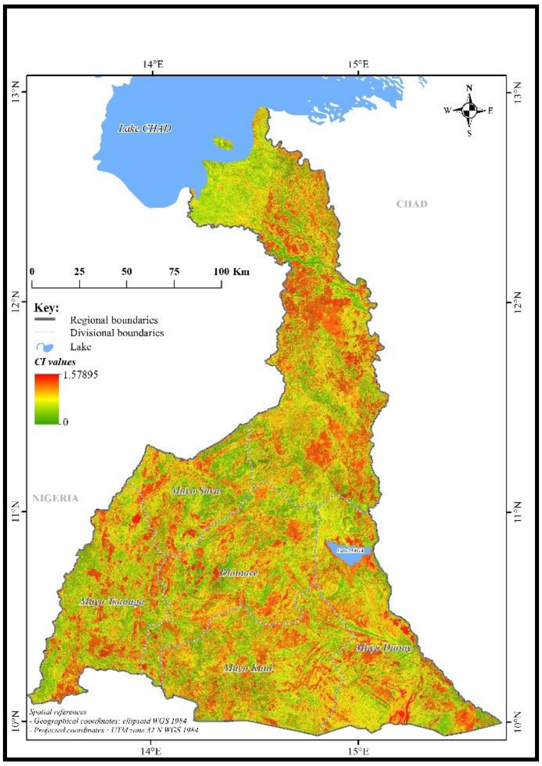

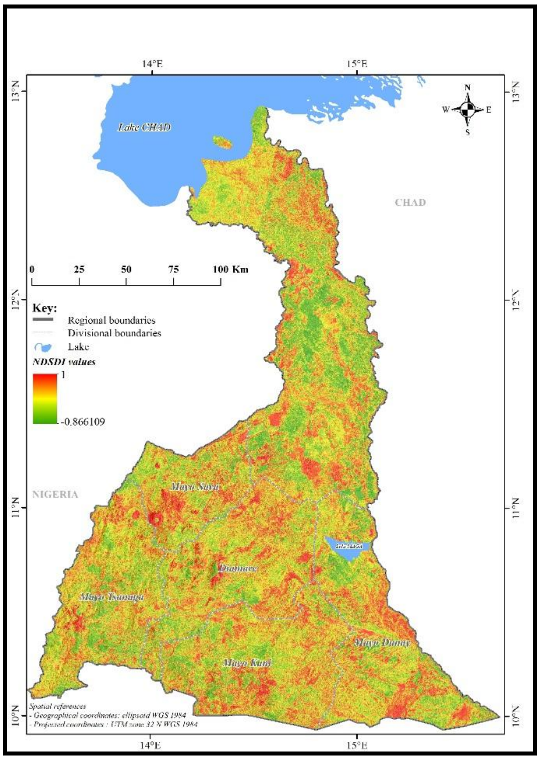

Figure 5c: *CI (vi)* *NDSDI (vii)*

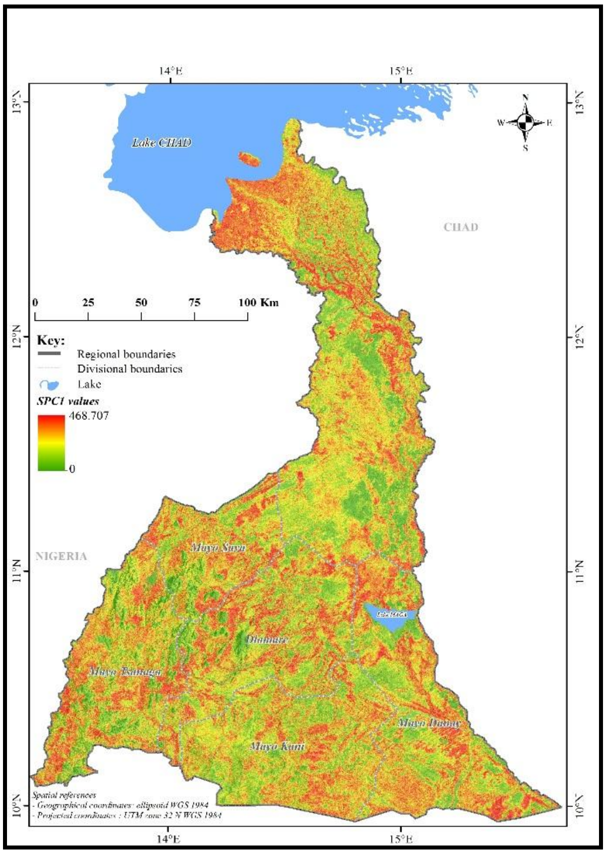

Figure 5d: *SPC1*

After it has been proceeded to a comparison between each index and SCP1 $_{\text{R-NIR-SWIR1-SWIR2}}$ on one hand as the dependent variables, with the MSAVI2 on the other hand as the independent variable. This was done considering the lack of vegetation as the first indicator of soil exposition to degradation. The comparison was made by the method of simple linear regression. The goal of this statistic method is to determine the equation model of the line that fit better the observed points in an (x, y) plan (Dagnelie, 2009). The equation is generally presented in the form:

$$y = ax + b$$

A correlation test has been also calculated to show the level of that linear relation between the others neo-bands and the MSAVI2. It just appears that the SCP1$_{\text{R-NIR-SWIR1-SWIR2}}$ is most strongly determined by the MSAVI2 with a coefficient of determination R^2 up to 0.3134 (Figure 6, Table 4). Also the highest negative correlation coefficient with the MSAVI2 is the SCP1$_{\text{R-NIR-SWIR1-SWIR2}}$ up to -0.5599; while the highest positive value is the GSI with -0.4493 (Table 4). All the P-values generated are strictly less than 0.0001 (Table 4) and knowing that P-values less than 0.05 are often reported as “statistically significant” (Sellke et al., 2001) all the neo-bands are then important for the analysis process.

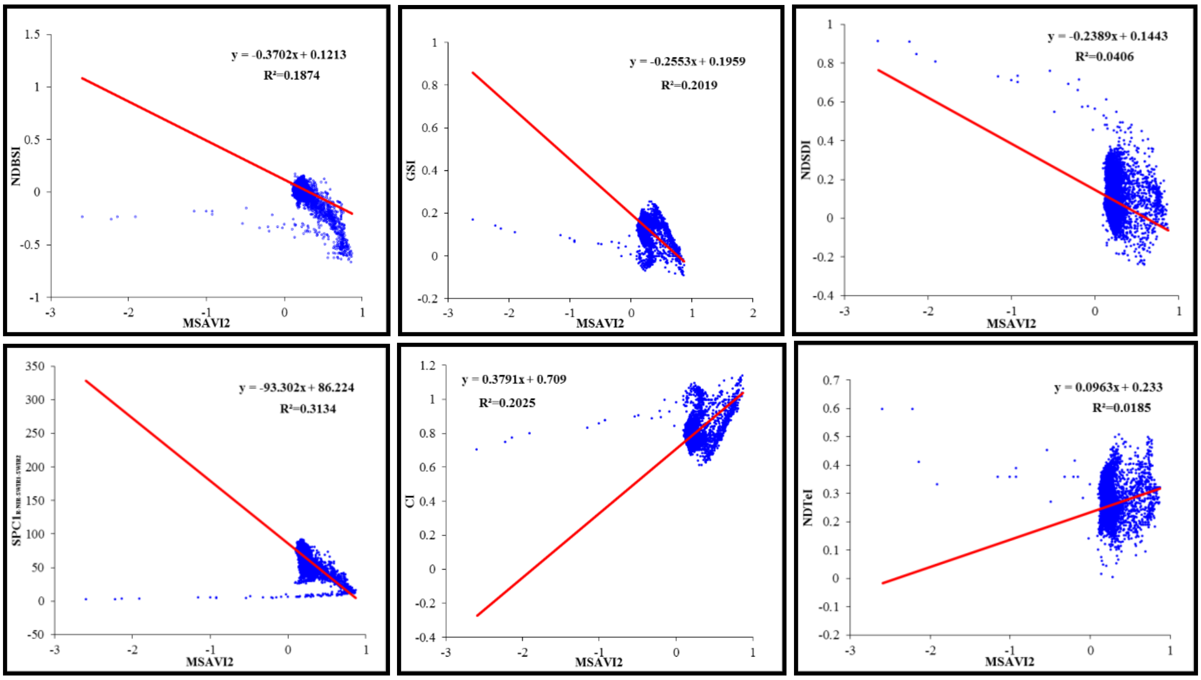

Figure 6: *The Correlation between MSAVI2 and the others Neo-Bands*

Table 4: *Statistic Relation between MSAVI2 and the others Neo-Bands*

Indicators of Correlation Neo-bands	Correlation Coefficient	Determination Coefficient R^2	P-values	
			Threshold	***Test***
NDBSI	-0.43271964	0.18740843	< 0.0001	Significant
NDTeI	0.13637548	0.01859827	< 0.0001	Significant
GSI	-0.44937944	0.20194188	< 0.0001	Significant
CI	0.45007158	0.20256443	< 0.0001	Significant
NDSDI	-0.20150989	0.04060623	< 0.0001	Significant
$SPC1_{R\text{-}NIR\text{-}SWIR1\text{-}SWIR2}$	-0.55990621	0.31349319	< 0.0001	Significant

2.3.2. The Neo-Bands Couples Reflectance Trends

The indices were grouped together in three pairs of indices according to their relation in characterizing land degradation (Figure 7). The visual overlay of the indices images generated can be observed and concluded on the basis of the contrast of reflectance values sampled for 40000 pixels distributed on all the features of bareness, roughness, encrusting, rough lithology, sand spread and implicitly a first pre-definition of degradation areas. The MSAVI2 appears then effectively negatively correlated to NDBSI, the contrast appearing therefore as a strong indicator of soil bareness. At same time GSI and NDTeI are also negatively correlated what supposes that they bring different additional information to enhance top soil texture. At last CI and NDSDI have a negative correlation and it is an indicator that any image adds different information to the model relatively to the encrusting and the sand.

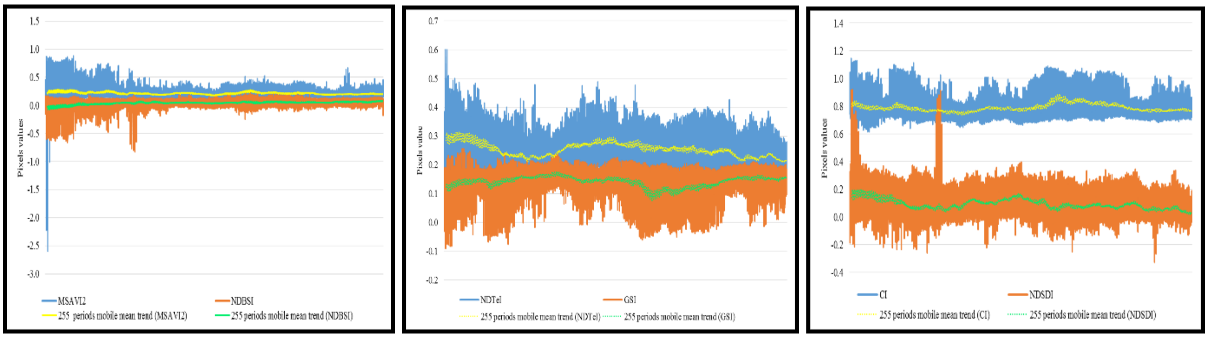

Figure 7: Reflectance Trends between the Three Couples of Spectral Indices

2.3.3. The Simple *Weighted Sum* Method

The indices were crossed following the weighted sum method. These were grouped together and crossed in three pairs of indices according to their relation and their explained proximity in characterizing the state of land degradation. They are each represented by six classes of information. Initially, the MSAVI2 and NDBSI were decomposed and crusaders with a view to characterize or confirm the state of soils bareness. This assumes in the synthetic image obtained that the low values of MSAVI2 correspond to high values of NDBSI to confirm the bare surfaces (Table 5). After the NDTeI and the GSI were crossed to appreciate the soil texture in terms of surface undulations and grain size. In this case, the six classes of these indices and the synthetic image obtained reflect the strong values to the coarser texture and low values for the less pronounced texture (Table 5). Furthermore the CI and the NDSDI were crossed to highlight areas of high attendance and sand crusts together. It therefore appears that the synthetic image spring for high values highly silted areas and much encrusted resulting high values of two crossed indices (Table 5). At last the three images obtained have been crossed with the $SPC1_{R\text{-}NIR\text{-}SWIR1\text{-}SWIR2}$ to obtain a synthetic image. This allowed a first assessment of the state of land degradation.

Table 5: Numerical Interpretation of the Weighted Sum Algorithm

Level of Degradation Indices for Degradation	Low					High
MSAVI2 (High to low vegetation cover)	0.958 – 0.354	0.354 – 0.165	0.165 – - 0. 023	-0.023 – -0.439	-0.439 – -1.271	-1.271 – -8.678
NDBSI (Low to high soil bareness)	- 0.999 – - 0.349	-0.349 – -0.176	- 0.176 - - 0.066	-0.066 – 0.011	0.011 – 0.082	0.082 – 0.999
NDTeI (Low to high soil texture and roughness)	- 1 – 0.043	0.043 – 0.145	0.145 – 0.223	0.223 – 0.286	0.286 – 0.372	0.372 – 1
CI (Low to high soil encrusting)	0 – 0.743	0.743 – 0.804	0.804 – 0.873	0.873 – 0.947	0.947 – 1.034	1.034 – 1.572
GSI (Low to high soil grain size and texture)	- 0.574 – - 0.037	- 0.037 – - 0.024	- 0.024 – 0.080	0.080 – 0.123	0.123 – 0.166	0.166 – 0.993
NDSDI (Low to high sand spread)	- 0.866 – - 0.119	-0.119 – 0.004	0.004 – 0.092	0.092 – 0.187	0.187 – 0.319	0.319 – 1
$SPC1_{R\text{-}NIR\text{-}SWIR1\text{-}SWIR2}$ (Low to high soil roughness)	0 – 20.218	20.218 – 34.923	34.923 – 49.627	49.627 – 64.332	64.332 – 104.769	104.769 – 468.706

2.3.4. The *Weighted Overlay Sum* Method

In ArcGIS 10.2.2 software this method uses proportion as percentages. The image resulting from the weighted sum crossing has been analyzed statistically. The linear regression has been once more used for this purpose (Figure 7). The objective has been to improve the contribution of any neo-band to the pre-detection of degraded lands. On the basis of the R^2 generated on the scatterplot it is observed that the synthesis image is more determined by the $SPC1_{R\text{-}NIR\text{-}SWIR1\text{-}SWIR2}$ up to 99.99%, contrarily to NDSDI that slightly determined it to 7.42% (Figure7, Table 6). Therefore the last step of the analysis was to weight of each index or neo-band by its determination coefficient R^2 with the synthesis image in order to enhance its contribution in the land degradation detection model and minimize any bias. The resulting image is considered optimal for contextual sensing of land degradation in arid and semi-arid regions.

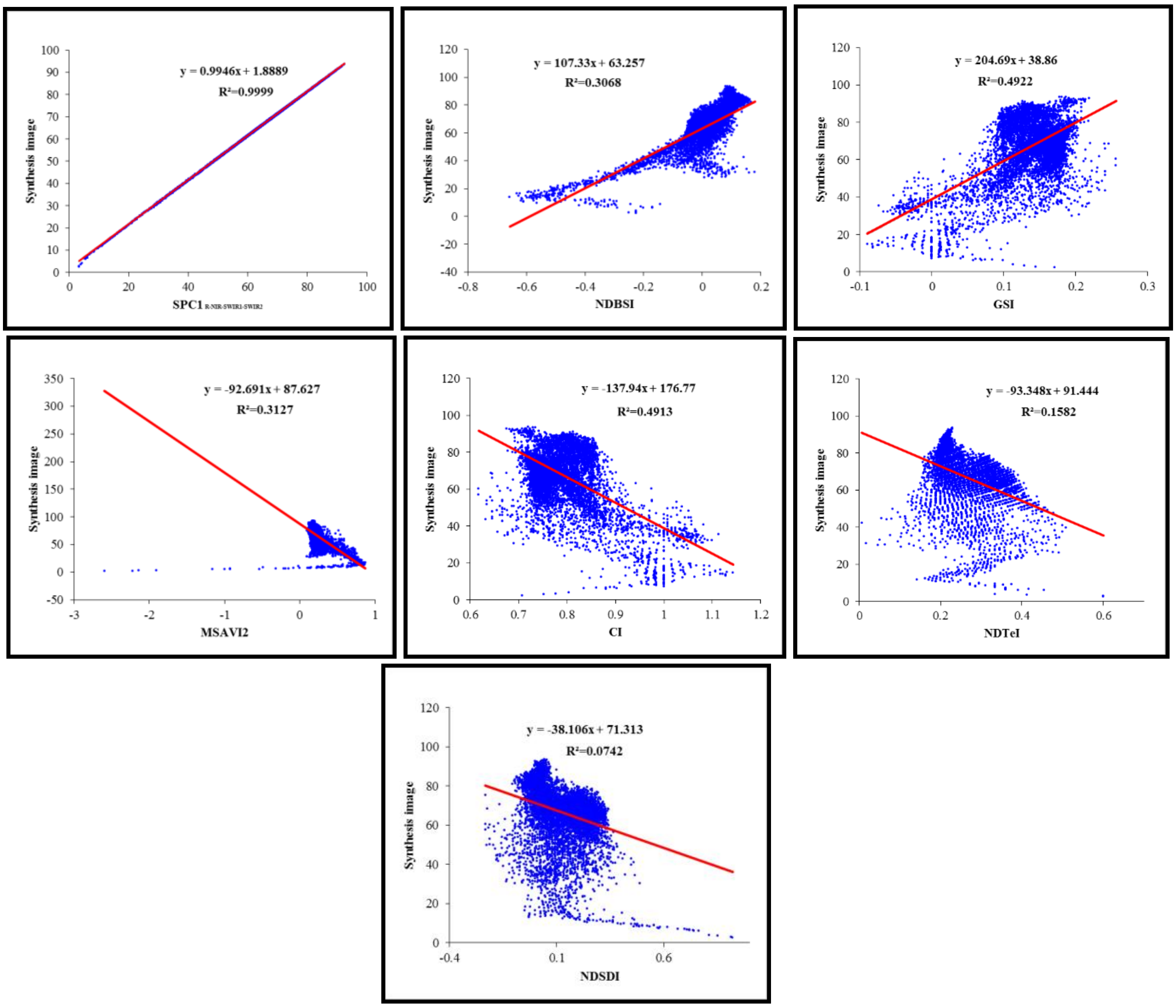

Figure 7: *The Correlation between the Synthesis Image and the Neo-Bands Crossed*

Table 6: *Statistic Relation between Synthesis Image and the others Neo-Bands*

Indicators of Correlation Neo-bands	Linear Model Full Equation (a + bx)	Determination Coefficient Full Value (R^2)	P-values	
			Threshold	*Test*
MSAVI2	63.256523+107.328965*0.107784	0.31271896	< 0.0001	Significant
NDBSI	87.627229-92.690587*0.187408	0.30680340	< 0.0001	Significant
NDTeI	91.443515-93.347721*0.225165	0.15823584	< 0.0001	Significant
GSI	38.859672+204.694035*0.085173	0.49221143	< 0.0001	Significant
CI	176.771284-137.941105*0.874418	0.49130331	< 0.0001	Significant
NDSDI	71.312706-38.105661*0.016806	0.07428657	< 0.0001	Significant
$SPC1_{R\text{-}NIR\text{-}SWIR1\text{-}SWIR2}$	1.888909+0.994648*77.067878	0.99993701	< 0.0001	Significant

2.4. The Analysis of Exposition to Degradation

The increase in population is one of the significant factors that influence and accelerate land degradation by creating a great pressure on the land and other natural resources (Fadhil, 2009). The villages and population layers point format of the study area has been used to perform this step of the process. The analysis has been performed via ArcGIS 10.2.2 software toolbox. The first part has consisted to convert the considered layers into density of surface using the *point density* function of *spatial analyst tool*. It calculates a magnitude per unit area from point features that fall within a neighborhood around each cell. Afterwards the result obtained has been reclassified to six classes and crossed to the image of degradation. The image obtained is the one considered as the decision or action map for government concerning the fight against arid land degradation. A general diagram resumes the methods used in this study (Figure 9).

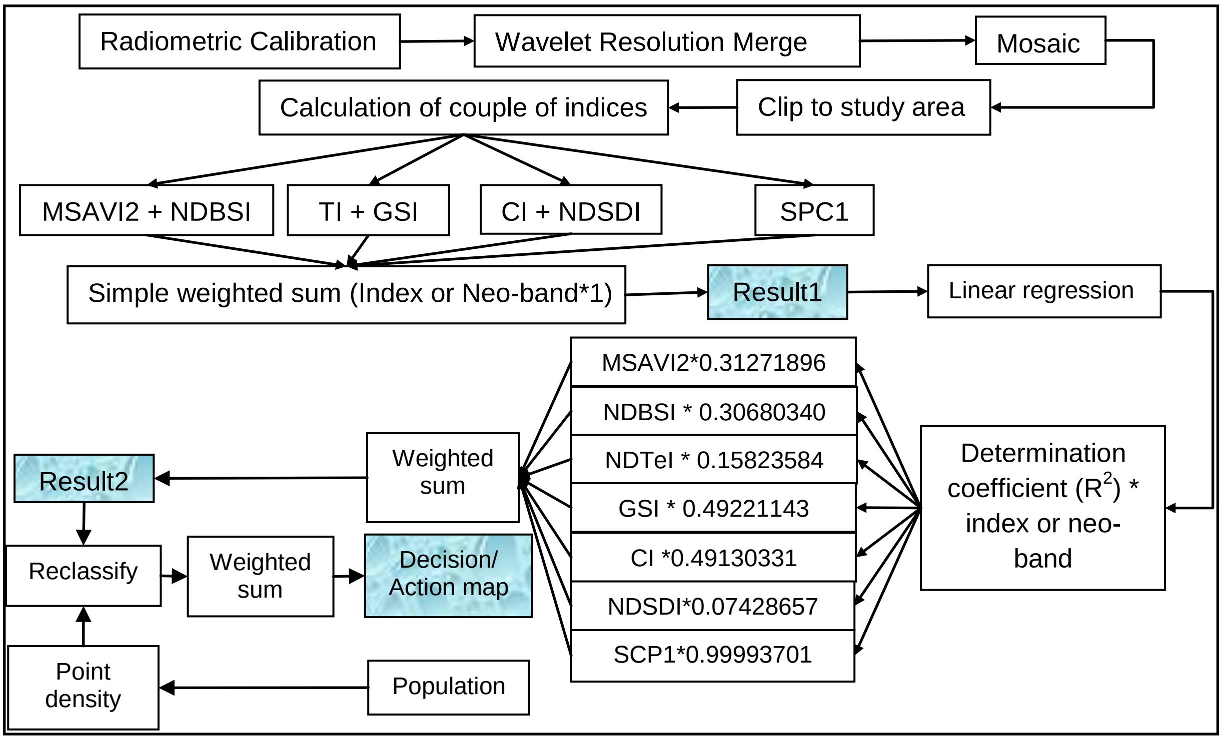

Figure 9: *Flowchart Illustrating the Methodology*

3. Results

3.1. Visual and Statistical Patterns of the Degradation Image

The results show six classes of land degradation on a nominal decreasing graduated scale that is arranged from the severe to the nil (Figure 10). The first remark is that a visual and statistic close relation between $SPC1_{R\text{-}NIR\text{-}SWIR1\text{-}SWIR2}$ and the degradation image; and this is confirmed by comparing the areas on each image class of degradation. Then the areas are evaluated respectively for SPC1 and resulting image to 3796 and 3139 km^2 for the class “severe”; 7483 and 6763 km^2 for the class ‘’high’’; 7984 and 8341 km^2 for the class ‘’moderate’’; 7424 and 7454 km^2 for the class ‘’low’’; 6291 and 6947 km^2 for the class ‘’very low’’; 5101 and 5437 km^2 for the class ‘’close to nil’’ (Table 7, Figure 10).

Likewise the total areas per indices and neo-bands have shown slight difference in total areas concerned by degradation. The most important difference is recorded between $SPC1_{R\text{-}NIR\text{-}SWIR1\text{-}SWIR2}$ and NDSDI; that is a residual of 9 km^2.

The quality of the model can also be analyzed still based on the areas per class for the different spectral and statistical neo-bands. It thus appears for the class "severe" that the MSAVI2 and the GSI with respectively 12235 km^2 and 5644 km^2 (Table 7, Figure 10) are the more explained; what probably indicates that the largest areas of bares soils severely degraded are constitutes from top soil grains size sandy or rocky humanly directly unusable. With 3139 km^2, the degradation image respectively 25.65% and 55.61% of MSAVI2 and GSI, explaining that all the vegetative uncover, sandy and rocky surfaces of this class are not degraded. The class ''high'' shows that the indices MSAVI2 and NDBSI with 20212 km^2 and 12661 km^2 more influences the model and thus lack of vegetation and bareness are the two main causes of degradation. The degradation image value recorded for this class is 6763 km^2, corresponding respectively to 33.46% and 53.41% of degraded land in MSAVI2 and NDBSI. For the class ''moderate'', NDTeI and NDSDI have the more large areas, respectively 12156 km^2 and 11113 km^2 which supposes that roughness and sand spread are the main causes of degradation at this level. The portion of degraded land expressed by the degradation image for this class is 8341 km2 that is 68.61% and 75.05% of the NDTeI and NDSDI. The class ''low'' is more represented by the NDSDI and CI, with respectively 9909 km^2 and 9057 km^2 and the two main causes of degradation are then sand spread and encrusting. The total of land degraded expressed by the degradation image is 7454 km^2 that is 75.22% and 82.30 % of the NDSDI and CI. The class ''very low'' records the more highest areas values from CI and $SPC1_{R\text{-}NIR\text{-}SWIR1\text{-}SWIR2}$ respectively 11946 and 6291 km^2; that supposes the importance of encrusting and rough lithology for this class. The degradation image for this class is 6947 km2, representing 58.15% and 110.4 % of the CI and the $SPC1_{R\text{-}NIR\text{-}SWIR1\text{-}SWIR2}$. At last the "close to nil" class shows that the $SPC1_{R\text{-}NIR\text{-}SWIR1\text{-}SWIR2}$ and the CI with respectively 5101 km^2 and 4020 km^2 record the highest areas which supposes that rough lithology and encrusting enhanced by these two neo-bands slightly influences the state of soil degradation in the study area. Comparatively to the degradation image which scored 5437 km^2 for this class it represent 106.5% and 135.2% for $SPC1_{R\text{-}NIR\text{-}SWIR1\text{-}SWIR2}$ and CI.

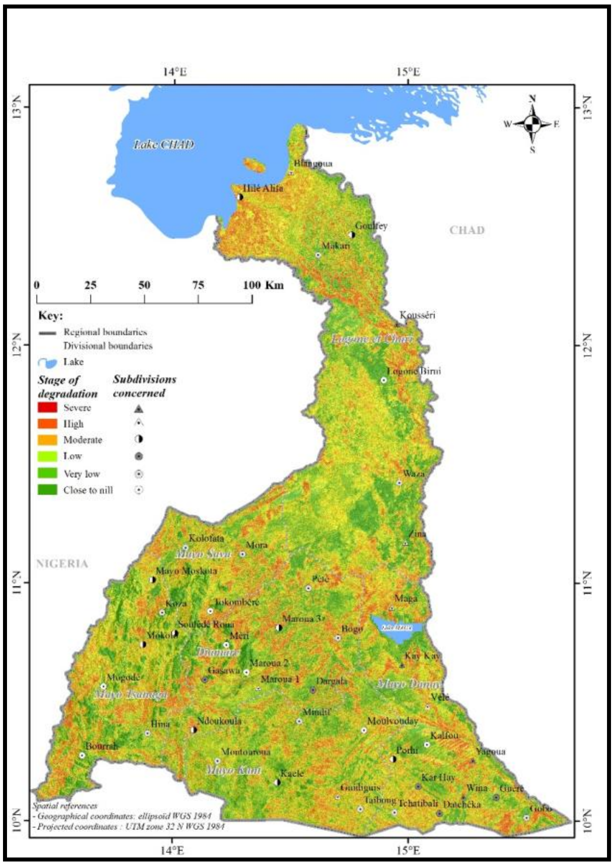

Figure 10: *Land Degradation Image*

Table 7: *Degraded Areas per Neo-Bands and Per Classes*

Neo-bands Classes	MSAVI2	NDBSI	GSI	NDTeI	CI	NDSDI	SPC1	Crossed Image	Two Main Causes of Degradation
Severe	12235	3642	5644	4222	1711	2590	3796	3139	Bareness and top soil grain size
High	20212	12661	12434	10718	5193	6624	7483	6763	Fallow and roughness
Moderate	4379	11090	7540	12156	6159	11113	7984	8341	Roughness and sand spread
Low	842	6925	6715	7246	9057	9909	7424	7454	Sand spread and encrusting
Very low	394	3019	4617	2712	11946	5961	6291	6947	Encrusting and rough lithology
Close to nil	20	751	1137	1032	4020	1889	5101	5437	Rough lithology and encrusting
Total	**38082**	**38088**	**38087**	**38086**	**38086**	**38086**	**38079**	**38081**	

3.2. Human Exposition and Spaces of Public Action

The vulnerability map obtained after crossing population density with degradation map shows that some spaces principally those dominated by the severe, high and moderate class of degradation have the priority of government action to initiate land rehabilitation and protection (Figure 11). The first is situated between the three departments of Diamare, Mayo-Sava and Mayo-Tsanaga. The second is mainly between the departments of Mayo-Kani and Mayo-Danay around the “duck-beak” very important for irrigated rice cultivation. The third area is situated in the division of Logone-Chari around the Lake Chad concerned with desertification and conflicts about land and water access.

The statistics extracted show that 279293 inhabitants live within the surface severely damaged (Table 8). At same time 548418 inhabitants are slightly concerned by the degradation (Table 8). When taking in consideration administrative limits of divisions, two of them are severely concerned by the degradation, notably the Mayo-Danay and the Logone-Chari, with respectively 178047 and 101246 inhabitants (Table 8).

Table 8: *Population Exposition per Class of Degradation and Per Administrative Division*

Division Classes	Diamare	Mayo-Danay	Mayo-Kani	Mayo-Sava	Mayo-Tsanaga	Logone-Chari	Total per class
Severe	0	178047	0	0	0	101246	**279293**
High	330410	126793	43632	0	0	75970	**576805**
Moderate	32091	0	144313	0	307310	218278	**701992**
Low	51296	112836	0	0	0	0	**164132**
Very low	132355	85182	134333	257634	124831	198017	**932352**
Close to nil	86834	26203	82368	91256	201490	331242	**819393**
Total per division	**632986**	**529061**	**404646**	**348890**	**633631**	**924753**	**3473967**

4. Discussions

Nevertheless other field components can interfere with the indices results such as landscape position (Demattê and al., 2009) and that effects are to be reduced. While in regions with a varied topography, elements as slope length and inclination named as LS factor in the USLE (Wischmeier and Smith, 1978) and RUSLE (Renard and al., 1991) formula are relevant to be introduced into the model. This is important to minimize and even subtract spectral values of each index due to the relief, when enhancing at same time some features of soil degradation.

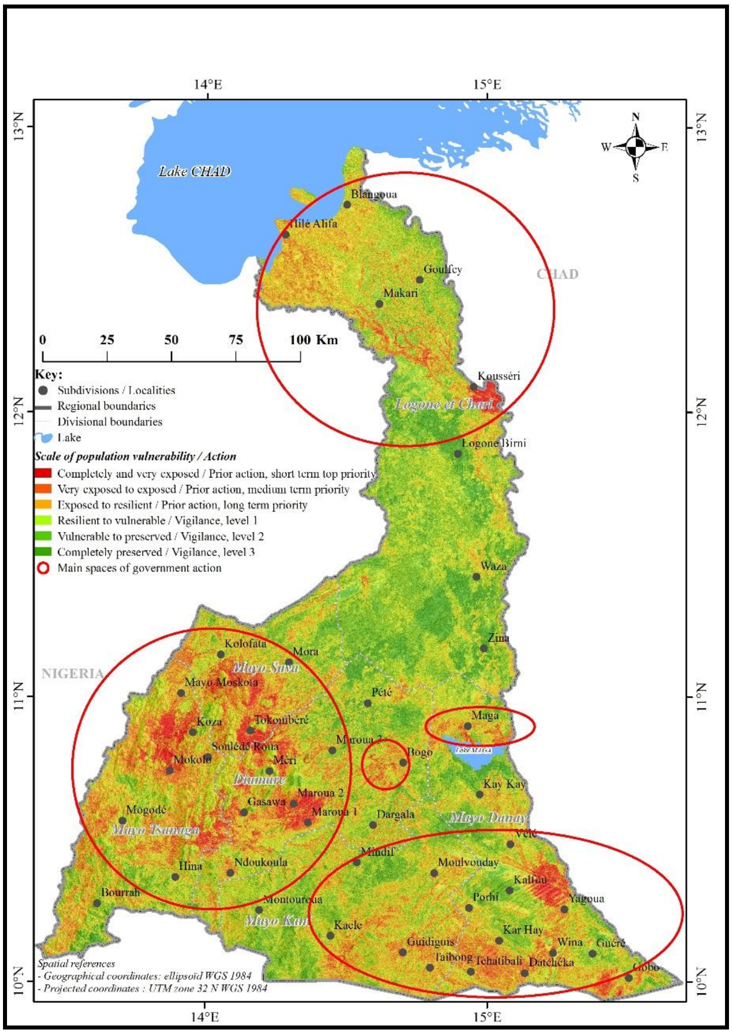

Figure 11: *People Exposition Map to Degradation*

Another bias can be introduced by human settlements like houses in sand materials and straw roof. These building materials strongly impact the top soil reflectance and can influence the values of indices to falsify the results of land degradation detection. No method has used to avoid such confusion during this experimentation.

Further apart from measuring and characterizing the degradation in laboratory before a deep field campaign verification it can also be important to integrate new instruments as mobile and portable spectroradiometers that have not been used in this study. They can facilitate a more precise measure of soil reflectance, color and composition (Escadafal et al., 1993), for a complementary comment on its degradation and the different noises and speckle around.

5. Conclusions

On the basis of laboratory test performed in this paper it is possible to detect the state of soil degradation in a semi-arid and arid tropical zone through the calculation and the crossing of spectral indices and statistical neo-band. Then the remote sensing techniques used are based on the visual and statistical comparison on one hand, and crossing of vegetation and soil indices with a statistical neo-band on the other hand to result in generating the land degradation image. The indices used in this study are MSAVI2, NDBSI, NDTeI, GSI, CI and NDSDI, and $SPC1_{R\text{-}NIR\text{-}SWIR1\text{-}SWIR2}$. And the generated index has been used to improve the accuracy of land degradation with regard to enhance characteristics as bareness, texture, roughness, sand spread and encrusting in arid and semi-arid zone.

Considering the soil cover or bareness as the first entrance, a vegetation index adapted to the area of study has to be calculated and correlated with the soil and top soil indices indicators of degradation. Thus the MSAVI2 has been correlated with the others neo-bands. Their p values obtained were strictly lower than 0.0001, and appeared then significant for the analysis. After they were summed following a simple weighted sum method a linear regression has been performed between every of them and the resulting image to assess the contribution of any neo-band to the model. Then each index or neo-band was weighted by its determination coefficient R^2 with the synthesis image in order to enhance its contribution and minimize any bias in the degradation image building model. It then appears that the final image corresponding to the degradation image is visually and statistically highly correlated to $SPC1_{R\text{-}NIR\text{-}SWIR1\text{-}SWIR2}$.

Nevertheless this experimentation has some limitations. The first one is the unused of the slope because of the plain relief in the study areas; which supposes that in topographic varied areas these elements are to be integrated in the model. In second point the sand materials and straw roof buildings can introduce bias in some indices calculation as NDSDI in desert and Sahel regions as the study areas; a method to avoid these confusion have to be found. The accuracy of the degradation image can be improved by field experimentations based on portable spectroradiometers.

Acknowledgments

The authors gratefully acknowledge the material and technical assistance of the National institute of cartography. The discussions with the technical members of the laboratory of image processing of the association ILG (I Love Geomatics) as well as those of the private consulting firm GEOVECTORIX are to be noted for the improvement of the content of this paper. The authors also highly appreciate all the facilities offered by the public administrations as Ministry of Environment, Nature protection and Sustainable Development, and the Central Bureau of Population Census concerning all the data provides.

Author Contributions

Alfred Homère NGANDAM MFONDOUM is the main author who co-initiated the idea and wrote the manuscript. Joachim ETOUNA co-initiated the idea, provided review and comments.

MBUJI Kindness Nongsi, Fabrice Armel MVOGO MOTO, and Florine Gustave NOULAQUAPE DEUSSIEU have contributed to technical processing and discussions.

References

Al-Bakri, J., Saoub, H., Nickling, W., Suleiman, A., Salahat, M., Khresat, S., and Kandakji, T. *Remote Sensing Indices for Monitoring Land Degradation in a Semiarid to Arid Basin*. In Jordan. Proc. of SPIE. 2012. 8538; 1-10.

Baccini, A. *Statistique Descriptive Multidimensionnelle*. Publications de l'Institut de Mathématiques de Toulouse, mai. 2010. 33.

Bai, Z.G., Dent, D.L., Olsson, L., and Schaepman, M.E., 2008: *Global Assessment of Land Degradation and Improvement 1. Identification by Remote Sensing*. In: GLADA Report 5, Version November 2008. 78.

Baraldi, A., Puzzolo, V., Blonda, P., and Bruzzone, L., and Tarantino C. *Automatic Spectral Rule-Based Preliminary Mapping of Calibrated Landsat TM and ETM+ Images*. IEEE Transactions on Geoscience and Remote Sensing. 2006. 44 (9) 2563-2586.

Barnes, R.A., and Zalewski, E.F. *Reflectance-Based Calibration of SeaWiFS-II.* Conversion to Radiance. Applied Optics. 2003. 42 (9) 1648-1660.

Barrow, C.J., 1991: *Land Degradation: Development and Breakdown of Terrestrial Environments*. Cambridge University Press, Cambridge, UK. 300.

Begzsuren, S., 2007: *Integrated Desertification Assessment in Southern Mongolia.* Dr. Thesis, University of Bonn. 141.

Biancalani, R. No Year: *Land Degradation Assessment in Drylands*. LADA Team, FAO-UNEP. 46.

Blaikie, P., and Brookfield, H., 1987: *Land Degradation and Society*. Methuen, London. 296.

Bonn, F., and Rochon, G., 1992: *Précis de télédétection*. Vol.1. Principes et méthodes. Ed. AUPELF-UREF, Presses Universitaires du Québec, Montréal.

Brabant, P., Darracq, S., Égué, K., and Simonneaux, V., 1996: *Togo: Human-Induced Land Degradation Status – Explanatory Notes on the Land Degradation Index*. ORSTOM editions, Paris 66.

Brabant, P. *A Global Land Degradation Assessment and Mapping Method. A Standard Guideline Proposal*. Les Dossiers Thématiques du CSFD. July 2009. (8) 2.

Brabant, P. *Une Méthode D'évaluation Et De Cartographie De La Dégradation Des Terres. Proposition De Directives Normalisées*. Les dossiers thématiques du CSFD. Août 2010. (8) 52.

BUCREP, 2010: *Rapport De Présentation Des Résultats Définitifs.* BUCREP, Cameroun, 22 avril 2010. 67.

Chavez, Jr. P.S. *Image-Based Atmospheric Corrections - Revisited and Improved*. Photogrammetric Engineering & Remote Sensing. 1996. 62 (9) 1025-1036.

Chen, Y., 1999: *Correlation of Saltbush Cover Measurements to TM Wavebands and Vegetation Indices.* Geoscience and Remote Sensing Symposium, IEEE IGARSS '99.

COMIFAC-CEEAC, 2007: Programme D'Action Sous-Régional de Lutte Contre la Dégradation des terres et la Désertification en Afrique Centrale (PASR/LCD–AC). Jun 2007, 65. Available on www.unccd.int/ActionProgrammes/rms-fre2007.pdf

Conacher, J., and Sala Wiley, M., 1998: *Land Degradation in Mediterranean Environments of the World: Nature and Extent, Causes and Solutions*. Chichester. 491.

Dagnelie, P. *De La Régression Linéaire Simple Et L'analyse De La Variance Aux Modèles Linéaires Généralisées: Synthèse Et Chronologie*. Revue MODULAD. 2009. 39; 107-136.

Demattê, J.A.M., Huete, A.R., Laerte Guimarães, F. Jr., Nanni, M.R., Alves, M.C., and Ricardo Fiorio, P. *Methodology for Bare Soil Detection and Discrimination by Landsat TM Image*. The Open Remote Sensing Journal. 2009. 2; 24-35.

Deschamps, P.Y., Duhaut, P., Rouquet, M.C., and Tanre, O., 1983: *Mise En Évidence, Analyse Et Correction Des Effets Atmosphériques Sur Les Données Multispectrales De Landsat Ou Spot.* Inra-CNES. Coll. Int. Signatures spectrales d'objets en Télédétection, Bordeaux, France. 709-722.

ERDAS, 2003: *ERDAS Field Guide, Seventh edition*. Leica Geosystems, Atlanta, Georgia. 698.

Escadafal, R., Gouinaud, C., Mathieu, R., and Pouget, M. *Le Spectroradiomètre De Terrain: UN Outil De La Télédétection Et De La Pédologie*. Cah. Orstom, sér. Pédol. 1993. XXVIII (1) 15-29.

Fadhil, A.M. *Land Degradation Detection Using Geo-Information Technology for Some Sites in Iraq*. Journal of Al-Nahrain University. 2009. 12 (3) 94-108.

Ferreres Mora, L., Ruiz Fernández, L.A., Artero Verdú, F., and Soo Kyun, Ik. *Using a Wavelet Based Method for High Resolution Satellite Image Fusion*.
Available on http://www.cgat.webs.upv.es/bigfiles/Ferreres_et_al(SNRFAI01).pdf

González, E.P., and Rodríguez, P.G. *Use of Remote Sensing in Soil Degradation*. Boletín de la Asociación de Geógrafos Españoles. 2013. 61; 425-427.

Gonzalez, P.L. No Year: *L'Analyse en Composantes Principales (ACP)*. 37. Available on maths.cnam.fr/IMG/pdf/A-C-P-.pdf

Higginbottom, T.P., and Symeonakis, E. *Assessing Land Degradation and Desertification using Vegetation Index Data: Current Frameworks and Future Directions*. Remote Sens. 2014. 6; 9552-9575.

Joly, G., 1986: *Traitements Des Fichiers Images*. Collection Télédétection satellitaire, n°3, Paradigme, Caen. 137.

Karnieli, A. *Development and Implementation of Spectral Crust Index over Dune Sands*. Int. J Remote Sensing. 1997. 18 (6) 1207-1220.

King, R., and Wang, J., 2001: *A Wavelet Based Algorithm for Pansharpening Landsat-7 Imagery.* Proceedings of the Geoscience and Remote Sensing Symposium, IGARSS. 2; 849-851.

Klonus, S., and Ehlers, M., 2009: *Performance of Evaluation Methods in Image Fusion.* 12th International Conference on Information Fusion, Seattle, WA, USA. July 6-9, 2009. 1409-1416.

Liu, A., and Wang, J., 2005*: Monitoring Desertification in Arid and Semi-Arid Areas of China with NOAA-AVHRR and MODIS Data.* Geoscience and Remote Sensing Symposium. IEEE, IGARSS '05.

Madeira, J., Pouget, M., Bedidi, A., and Cervelle, B. *Relations entre les constituants minéraux d'Oxisols brésiliens et leurs signatures spectrales du visible à l'infra-rouge moyen: application à des données satellitaires (Landsat TM): I- Les oxydes de fer. - II. La kaolinite et la gibbsite. Implications sur la texture*. Télédétection, ORSTOM, Paris. 1991. 6.

Madeira, J., 1993: Etude qualitative des relations constituants minéralogiques-réflectance, diffusion des latosols brésiliens: applications à l'utilisation pédologiques des données satellitaires TM (région de Brasilia). Coll. Etudes et Thèses. Orstom éd. 1993. Paris. 236.

Metternicht, G., 2006: *Current Developments of Remote Sensing for Mapping and Monitoring Land Degradation at Regional Scale*. UN-Zambia-ESA Regional Workshop on the Applications of GNSS in Sub-Saharan Africa, Zambia. June 2006. 40.

Ministère de l'environnement et des forets (Cameroun), UNCCD, 2004: Rapport National sur la mise en œuvre de la convention des Nations Unies sur la lutte contre la désertification. Novembre 2004. UNCCD. 53.

Pandey, P.C., Rani, M., Srivastava, P.K., Sharma, L.K., and Nathawat, M.S. *Land Degradation Severity Assessment with Sand Encroachment in an Ecologically Fragile Arid Environment: A Geospatial Perspective*. In Q Science Connect. 2013. 43; 17.

Perry, C. Jr., and Lautenschlager, L.F. *Functional Equivalence of Spectral Vegetation Indices*. Remote Sensing of Environment. 1984. 14 (1-3).169-182.

Qi, J., Chehbouni, A., Huete, A.R., Kerr, Y.H., and Sorooshian, S. *A Modified Soil Adjusted Vegetation Index*. Remote Sens. Environ. 1994. 48; 119-126.

Raina, P., Joshi, D.C., and Kolarkar, A.S. *Land Degradation Mapping By Remote Sensing in the Arid Region of India*. Soil Use Manage. 1991. 7 (1) 47-51.

Raunet, M. *Quelques clés morphopédologiques pour le Nord Cameroun à l'usage des agronomes*. Cirad, France. September 1993. 21.

Renard, K.G., Foster, G.R., Weesies, G.A., and Porter, J.P. *RUSLE, Revised Universal Soil Loss Equation*. J. Soil Water Conserv. 1991. (1) 30-33.

Rojas, N., 2013: *An Overview of the Geospatial Methodologies used in Order to Assess the Soil Erosion Risk by Water.* Aplicaciones Espaciales de Alerta y Respuesta a Emergencias. February 2013. 41.

Roy, P., Miyatake, S., and Rikimaru, A. *Biophysical Spectral Response Modeling Approach for Forest Density Stratification*. ACRS 1997.
Available on http://www.a-a-r-s.org/aars/proceeding/ACRS1997/Papers/FR97-7.htm

Sellke, T., Bayarri, M.J., and Berger, J.O. *Calibration of P Values for Testing Precise Null Hypotheses*. The American Statistician. February 2001. 55 (1).

Smith, A., Freemantle, J., Nadeau, C., Wehn, H., Zwick, H., and J. Miller. 2005: *Leaf Area Index Map Generation Using CHRIS Data.* Presentation given at the 3rd CHRIS Proba Workshop. 2005.

Senseman, G.M., Bagley, C.F., and Tweddale, S.A. *Correlation of Rangeland Cover Measures to Satellite-Imagery-Derived Vegetation Indices*. Geocarto International. 1996. 11 (3) 29-38.

Senseman, G.M., Tweddale, S.A., Anderson, A.B., and Bagley, C.F., 1996: *Correlation of Land Condition Trend Analysis (LCTA) Rangeland Cover Measures to Satellite-Imagery-Derived Vegetation Indices.* US Army Corps of Engineers USACERL. Technical Report 97/07.

Singer, M.J., and Munns, D.N., 2002: *Soils: An Introduction.* 5th Edition. Upper Saddle River, New Jersey: Prentice Hall Publishers.

Thomasson, J.A., Sui, R., Cox, M.S., and Al-Rajehy, A. *Soil Reflectance Sensing for Determining Soil Properties in Precision Agriculture*. Trans. ASAE. 2001. 44 (6) 1445-1453.

Touriño Soto, I., 2005: *Mise En Relation De La Cartographie Du Rendement Avec La Distribution Spatiale De L'état De Surface Du Sol Observée Par Télédétection.* Application dans un contexte d'agriculture de précision. Th. Dr. L'Institut National Polytechnique de Toulouse. 259.

UNCCD, 1994: United Nations Convention to Combat Desertification in Those Countries Experiencing Serious Drought and/or Desertification, Particularly in Africa. UN, Paris, France.

UNEP, 1992: *World Atlas of Desertification.* Edward Arnold, London.

Warren, A., and Agnew, C. *An Assessment of Desertification and Land Degradation in Arid and Semi-Arid Areas*. Drylands Program, Issues Envelope. April 1998. 2.

Wischmeier, W.H., and Smith, D.D. 1978: *Predicting Rainfall Erosion Losses: A Guide to Conservation Planning*. USDA, Agriculture Handbook 537. U.S. Government Printing Office, Washington, DC.

Xiao, J., Shen, Y., Tateishi, R., and Bayaer, W. *Development of Topsoil Grain Size Index for Monitoring Desertification in Arid Land Using Remote Sensing*. Int. J. Remote Sensing. 2006. 27 (12) 2411-2422.

Youan, T.M., 2008: Contribution de la télédétection et des systèmes d'informations géographiques à la prospection hydrogéologique du socle précambrien d'Afrique de l'Ouest: Cas de la région de Bondoukou Nord Est de la Côte d'Ivoire. Thèse de doctorat unique, Université de Cocody-Abidjan (Côte d'Ivoire), 236.

Zaydan, A.H. *Using a Wavelet Based Method for High Resolution Satellite Image Fusion*. Iraqi Journal of Science. 2012. 53 (4) 999-1005.